

Observations of near-inertial current variability on the New England shelf

R. Kipp Shearman

Department of Physical Oceanography, Woods Hole Oceanographic Institution, Woods Hole, Massachusetts, USA

Received 23 February 2004; revised 13 August 2004; accepted 28 December 2004; published 17 February 2005.

[1] Observations from the Coastal Mixing and Optics (CMO) moored array (deployed from August 1996 through June 1997) and supplemental moored observations are used to describe near-inertial current variability over the New England shelf. Near-inertial band current variance comprises 10–20% of the total observed current variance, and has episodic peak speeds exceeding 30 cm s^{-1} . Near-inertial current variability during CMO is characterized by a first baroclinic mode vertical structure with one zero-crossing between 15 and 50 m. The zero-crossing is shallower during periods of stronger stratification. Laterally, near-inertial variability is coherent over the extent of the CMO moored array, and cross-shelf decorrelation scales for near-inertial currents are about 100 km, approximately the entire shelf width. The magnitude of near-surface near-inertial variability is stronger in the summer and weaker in the winter, following the seasonal variation in stratification and opposite the seasonal cycle in wind stress variance. During CMO, near-surface near-inertial kinetic energy is inversely related to surface mixed layer depth. Near-inertial variance decreases onshore, matching approximately the cross-shelf decrease in near-inertial energy predicted by a two-dimensional, linear, flat-bottom, two-layer, coastal wall model. In this model, the nullifying effects of a baroclinic wave emanating from the coastal wall play a dominant role in controlling the onshore decrease. Finally, strong persistent anticyclonic relative vorticity shifts near-inertial variability on the New England shelf to subinertial frequencies.

Citation: Shearman, R. K. (2005), Observations of near-inertial current variability on the New England shelf, *J. Geophys. Res.*, 110, C02012, doi:10.1029/2004JC002341.

1. Introduction

[2] Wind-driven near-inertial variability is a common feature of the midlatitude, upper-ocean current field, and many characteristics are well understood [Pollard, 1970, 1980]. In the coastal ocean, though, a number of circumstances create more complicated patterns to near-inertial variability, and the important physical processes are not always clear. Foremost, the presence of the impenetrable coastal boundary can cause divergence in the upper ocean flow, rapidly generating near-inertial currents below the mixed layer and leading to near-inertial variability with low modal vertical structure [Millot and Crepon, 1981; Pettigrew, 1981; Kundu et al., 1983; Tintore et al., 1995; Chen et al., 1996]. However, near-inertial variability similar to the open ocean case (i.e., surface intensified with downward propagation of energy) can also be found in the coastal ocean [Kundu, 1976; Chant, 2001; Lerczak et al., 2001]. In addition, fronts, current jets, and eddies, fundamental components of circulation over many continental shelves, potentially affect near-inertial variability via nonlinear interactions between the subtidal and near-inertial current fields

[Kunze, 1985; Federiuk and Allen, 1996; Young and Ben Jelloul, 1997].

[3] From August 1996 through June 1997, a mooring array was deployed on the New England shelf south of Cape Cod (Figure 1) as part of the Office of Naval Research sponsored Coastal Mixing and Optics (CMO) experiment [Dickey and Williams, 2001]. The broader objectives of the CMO experiment were to understand the processes that affect vertical mixing of physical and optical properties over the shelf. Observations from the CMO moored array are used here to examine the characteristics and dynamics of near-inertial variability on the New England shelf. Also, supplemental moored current observations from the 1979–1980 Nantucket Shoals Flux Experiment (NSFE) [Beardsley et al., 1985], the 1983–1984 Shelf Edge Exchange Processes study (SEEP) [Aikman et al., 1988], the 1995–1997 Shelfbreak Primer program [Fratantoni and Pickart, 2003], and the June–August 2001 Coupled Boundary Layers Air-Sea Transfer (CBLAST) [Weller et al., 2003] Experiment are used to place the CMO observations in a broader context.

[4] The dominant physical characteristics of the New England shelf are the marked seasonal change in stratification [Bigelow, 1933; Beardsley et al., 1985] and the presence of the shelf-slope front [Islen, 1936; Linder and Gawarkiewicz, 1998]. During the summer, New England

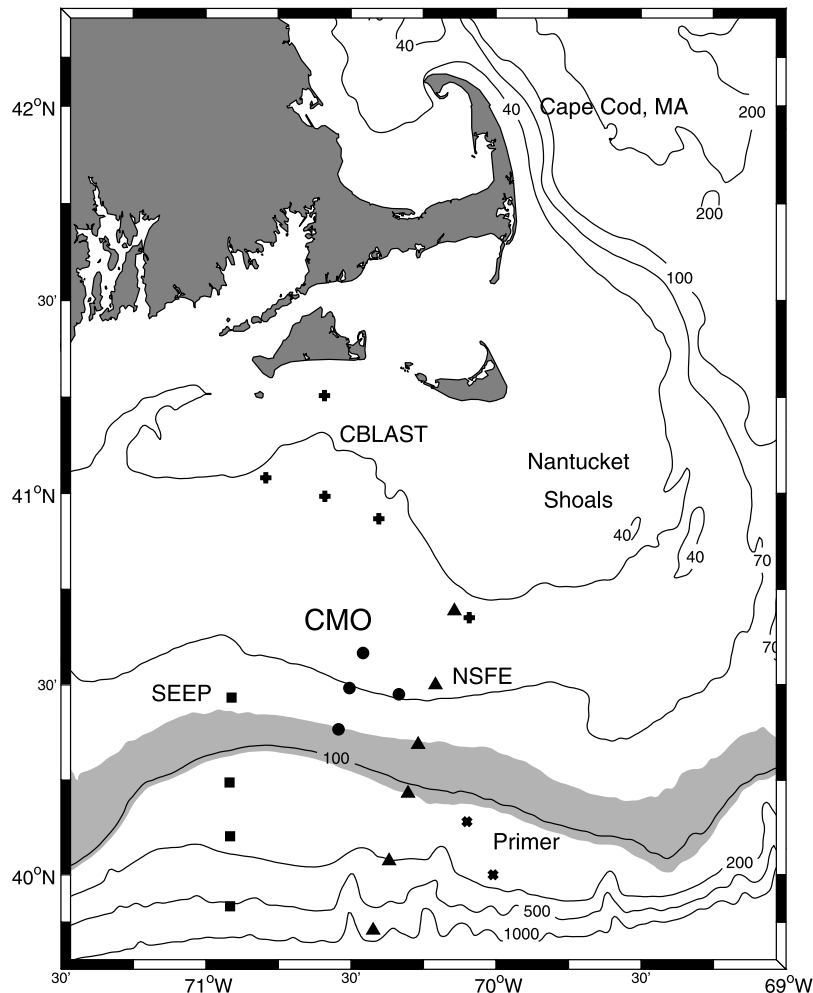


Figure 1. Location of the CMO moored array and bathymetry over the New England shelf. Seasonal range of the foot of the shelfbreak front as determined by *Linder and Gawarkiewicz* [1998]. Also shown are the locations of the NSFE, SEEP, CBLAST, and Shelfbreak Primer mooring sites.

shelf water is strongly stratified due to surface heating, while during the winter, shelf water is typically unstratified due to cooling and increased wind variability. This is generally true over the deployment of the CMO moored array except for a period in mid-winter when the shelf-slope front intrudes, introducing stratification lower in the water column [*Lentz et al.*, 2003]. The shelf-slope front is the boundary between relatively cool, fresh shelf water and warm, salty slope water, and the foot is typically found within 10–15 km of the 100-m isobath (see Figure 1) on the New England shelf [*Linder and Gawarkiewicz*, 1998]. There is strong westward subtidal geostrophic flow associated with the shelf-slope front [*Fratantoni and Pickart*, 2003], as well as weaker westward flow onshore of the front [*Shearman and Lentz*, 2003]. Thus there is a wide variety of stratification and subtidal flow conditions underlying near-inertial variability on the New England shelf. Wind forcing over the New England shelf is characterized by large-scale (700 km) low pressure systems, typically propagating from southwest to northeast along shelf and resulting in relatively uniform forcing conditions across the New England shelf [*Baumgartner and Anderson*, 1999].

[5] Previous descriptions of near-inertial current variability on the New England shelf indicated RMS currents of up to 10 cm s^{-1} and an on-shelf decrease in near-inertial current variance [*Beardsley et al.*, 1985]. A detailed examination found near-inertial current variability during NSFE to be mostly the result of wind forcing with large cross-shelf scales and a first baroclinic mode vertical structure [*Wood*, 1987]. A nearby study on the New York Bight identified near-inertial current variability after the passing of a hurricane with a first and second baroclinic mode vertical structure and some evidence of frequency shifting by the subtidal relative vorticity field [*Mayer et al.*, 1981]. In addition, more recent observations and analysis of wind-driven near-inertial variability on the New England shelf indicate low mode vertical structure, and a unique transfer of energy from the first to the second baroclinic mode, associated with bottom drag (J. A. MacKinnon and M. C. Gregg, Near-inertial waves on the New England shelf: The role of evolving stratification, turbulent dissipation, and bottom drag, submitted to *Journal of Geophysical Research*, 2005).

[6] The objectives of this paper are to characterize the magnitude, vertical structure, cross-shelf structure, and

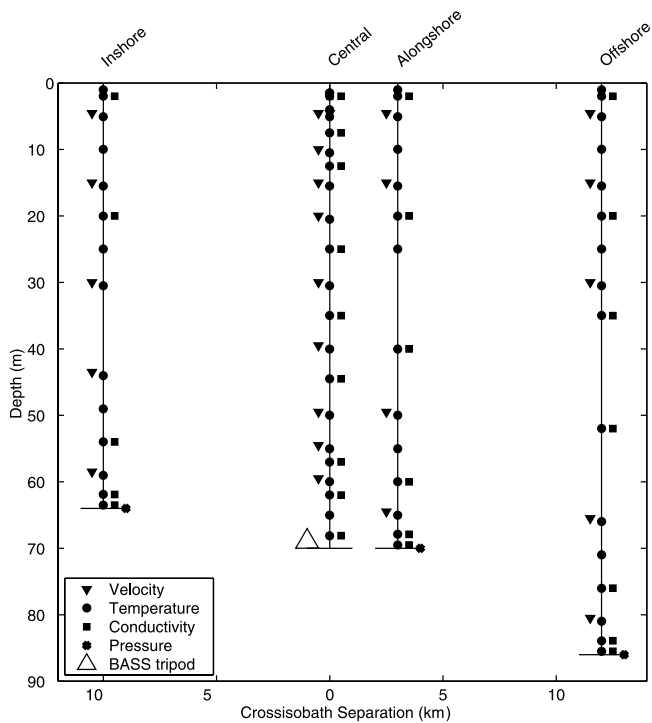


Figure 2. Subsurface instrumentation on the CMO moored array.

seasonal variability of near-inertial current variability on the New England shelf, and to understand the physical processes responsible for the cross-shelf distribution of near-inertial energy and the effects of the subtidal back-

ground flow on near-inertial motion. The remainder of the paper is organized as follows: Section 2 describes the CMO and supplemental moored observations, section 3 describes the basic characteristics of near-inertial variability on the New England shelf, section 4 discusses the cross-shelf distribution of near-inertial kinetic energy and the effects of subtidal flow on near-inertial motion, and section 5 summarizes the preceding material.

2. CMO Moored Observations

[7] The CMO moored array was deployed on the New England shelf approximately 100 km south of Cape Cod, Massachusetts, and just inshore of the average position of the foot of the shelf-slope front (Figure 1). This region of the New England shelf is oriented roughly east-west and is relatively broad (about 100 km wide), although the distance from the 40-m isobath to the shelfbreak (approximately the 150-m isobath) narrows to the east due to the presence of the Nantucket Shoals.

[8] The CMO moored array consisted of four sites, occupied continuously from August 1996 through June 1997. The central site was located at $40^{\circ}29.5'N$, $70^{\circ}30.5'W$ in 70 m of water, and the three surrounding sites (inshore, offshore, and alongshore) were located approximately 11 km inshore in 64 m of water, 12.5 km offshore in 86 m of water, and 14.5 km east along the 70-m isobath. All four sites included observations of currents, temperature, and conductivity, spanning the water column (Figure 2). In addition, the central site included high-quality observations of wind stress [Martin, 1998], and for a shorter duration (18 August to 27 September 1996, 7 October to 16 November 1996, and 17 April to 10 June 1997), direct covariance estimates of near bottom stress [Shaw *et al.*,

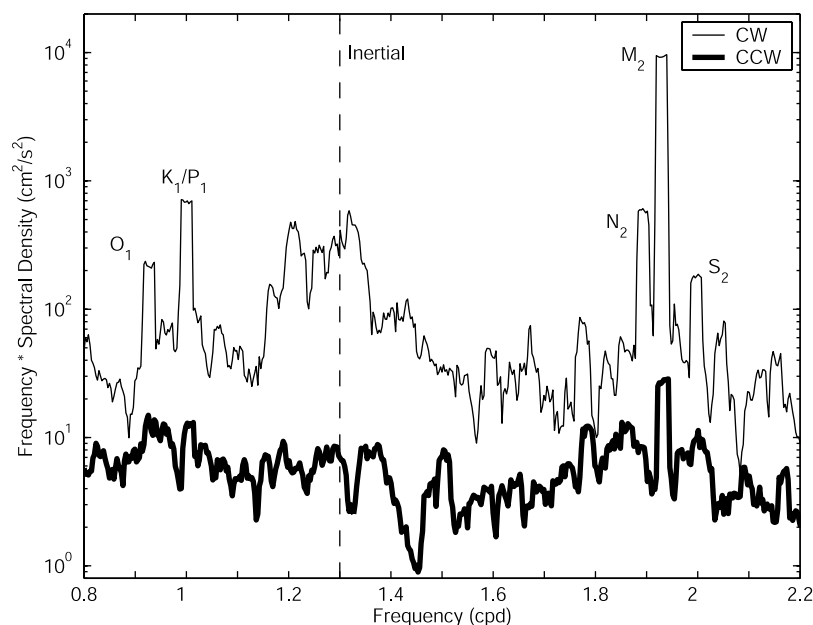


Figure 3. Variance preserving rotary spectra (clockwise, thin line; counterclockwise, thick line), computed from the 15-m central site vector-measuring current meter (VMCM) observations, over the tidal and inertial frequency range. The local inertial frequency is shown (dashed line), and individual tidal constituent peaks are labeled.

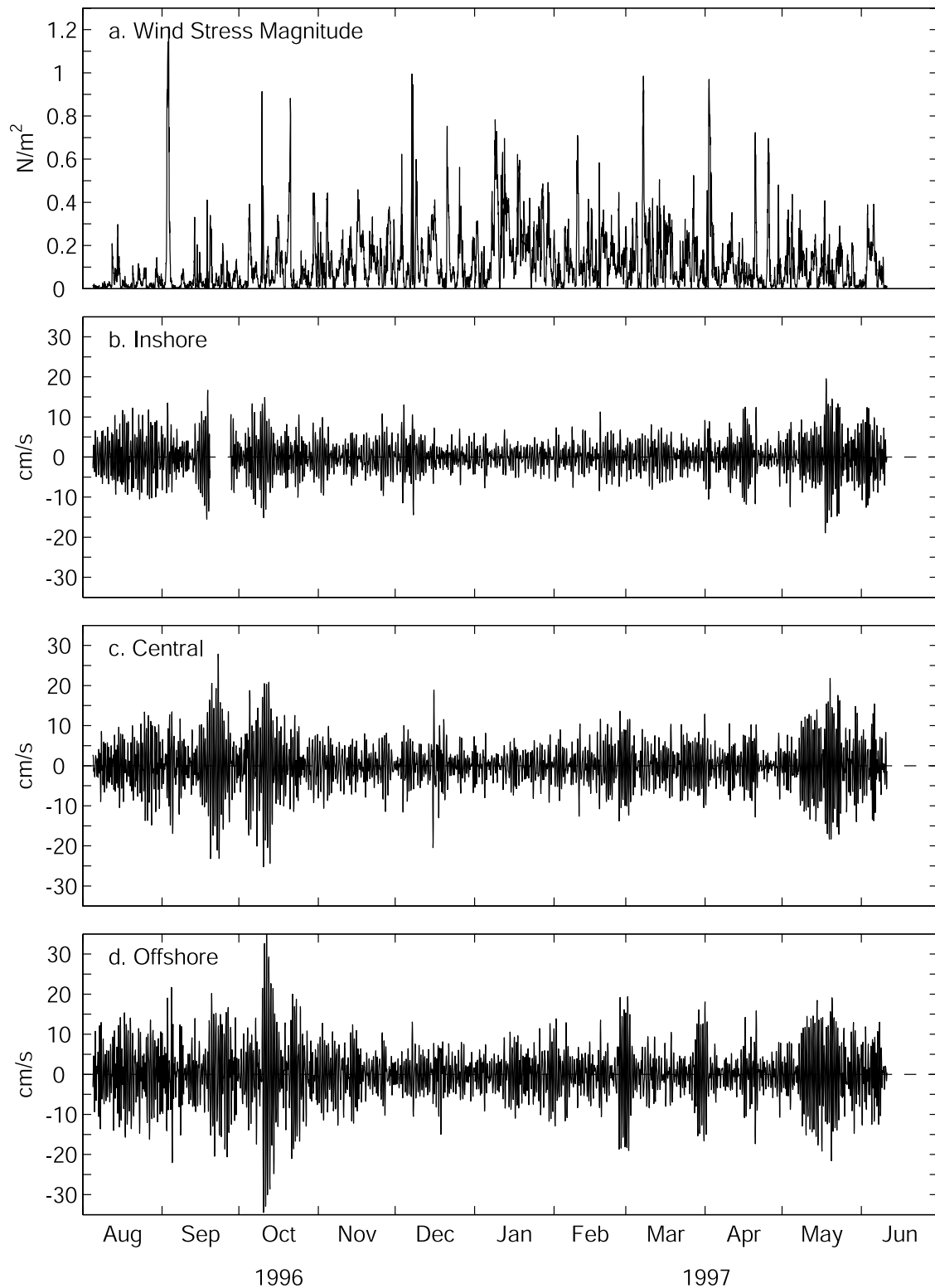


Figure 4. CMO moored observations of (a) wind stress magnitude and detided band-passed (10–33 hours) northward currents at 15 m for the (b) inshore, (c) central, and (d) offshore sites.

2001], made from velocimeters mounted on a bottom tripod [Williams *et al.*, 1987], the Benthic Acoustic Stress Sensor (BASS).

[9] A thorough description of the moored instrumentation, sampling strategies, and data processing techniques is

contained in the data report by Galbraith *et al.* [1999]. Moored current observations, during CMO, were made from 25 vector-measuring current meters (VMCMs) and two 300-kHz RD Instruments acoustic Doppler current profilers (ADCPs). The sample interval for VMCMs was

Table 1. List of Subjectively Identified Near-Inertial Events With the Peak Near Surface Kinetic Energy (KE) and Approximate Duration^a

Date	Max $ \tau $, N m ⁻²	Inshore		Central		Offshore	
		Max KE, cm ² s ⁻²	Duration, days	Max KE, cm ² s ⁻²	Duration, days	Max KE, cm ² s ⁻²	Duration, days
13 Aug. 1996	0.3	90	7.0	90	9.0	120	10.0
17 Sept. 1996	0.4	180	6.0	400	9.5	340	10.0
08 Oct. 1996	0.9	170	5.0	360	8.5	750	9.0
20 Oct. 1996	0.8	—	—	75	4.5	200	6.5
11 Nov. 1996	0.3	40	3.5	30	5.0	85	6.0
23 Nov. 1996	0.2	60	4.0	80	4.5	75	3.5
06 Dec. 1996 ^b	1.0	110	5.5	80	7.0	100	6.0
25 Dec. 1996	0.5	30	2.0	30	2.5	55	3.0
10 Jan. 1997	0.5	40	3.5	65	6.0	100	10
28 Jan. 1997	0.5	20	2.0	60	4.0	100	5.0
25 Feb. 1997	0.5	40	3.5	110	6.5	230	7.0
15 March 1997	0.4	30	3.5	65	4.0	100	4.0
14 April 1997	0.2	80	4.5	60	6.0	100	6.0
06 May 1997	0.3	50	9.0	90	9.5	130	10
16 May 1997	0.4	200	7.5	240	8.0	265	9.0
Mean	0.5 ± 0.1	81 ± 16	4.8 ± 0.5	122 ± 30	6.3 ± 0.6	183 ± 45	7.0 ± 0.6

^aAll events except one have a first baroclinic modal structure. All events are preceded by a change in wind stress forcing, and the peak wind stress magnitude preceding each event is reported. However, the detailed characteristics of wind forcing (i.e., rate of increase/decrease, turning direction, turning rate, etc.) are highly variable. Dashes denote that there is no apparent near-inertial variability at the inshore site.

^bNear-inertial variability had barotropic vertical structure (i.e., phase constant with depth).

7.5 min and for ADCPs was 3 min. The time series of raw current observations were filtered to remove variability at timescales less than 1 hour, and then decimated to hourly values. The accuracy of hourly current observations is estimated to be 2–3 cm s⁻¹ [Beardsley, 1987].

[10] Current vectors are analyzed in a coordinate frame where the positive x axis is oriented due east and the positive y axis is due north. However, it is important to note that the subtidal flow on the New England shelf is polarized along 110°T, which matches the along-isobath orientation of the bathymetry over length scales of 10–50 km [Shearman and Lentz, 2003].

3. Characteristics of Near-Inertial Variability on the New England Shelf

[11] Near-inertial variability is quite vigorous on the New England shelf. During CMO, the clockwise (CW) rotary spectra (Figure 3) are dominated by narrow-banded peaks at tidal frequencies and a broad-banded peak about the local inertial frequency of 1.3 cpd (spectra are qualitatively similar at all sites and depths). Near-inertial band (1.1–1.6 cpd) variability accounts for 10–20% of the total observed current variance during CMO (timescales ranging from 2 hours to 10 months) with rms values ranging from 2 to 9 cm s⁻¹. Near-inertial motions are thus the largest component of internal wave band current variability at the CMO site, an order of magnitude greater than the current variance associated with internal tides and high-frequency internal solitons [Shearman and Lentz, 2004]. Near-inertial band variance typically has a mid-depth minimum at about 30 m, and generally is smaller at the inshore site than at the central and offshore sites.

[12] To focus on near-inertial motions, barotropic tidal variability was removed using harmonic analysis [Shearman and Lentz, 2004], and the detided currents were band-passed to retain variability at timescales between 1 and 33 hours. The detided band-passed currents (Figure 4) are

dominated by inertial band variability, constituting about 80% of the variance, and the remaining variance is largely attributable to semidiurnal internal tides [Shearman and Lentz, 2004]. The detided band-passed currents exhibit bursts of near-inertial currents as large as 30 cm s⁻¹ that are stronger in the fall and spring than in winter. Principal axes, computed from the detided band-passed current observations, are nearly circular with ellipticities (ratio of minor to major axes) on average greater than 0.9 and no consistently preferred orientation.

[13] Bursts of near-inertial variability are usually preceded by a short duration wind event of varying magnitude (see Table 1 for a list of relatively large amplitude events). However, near-inertial current variability is highly intermittent, and not all substantial, short-duration wind events trigger near-inertial variability. For example, on 3 September 1996 when Hurricane Edouard passes the CMO site, the highest wind stress magnitude is observed, but little near-inertial current variability results (Figure 4). Previous studies on the continental shelf have used one-dimensional models forced by the observed wind stress to estimate the wind-driven contribution to near-inertial variability [e.g., Chen *et al.*, 1996], but for some coastal settings, two-dimensional processes may dominate [e.g., Millot and Crepon, 1981; Pettigrew, 1981], creating substantial differences in the wind-driven response (i.e., the rapid transfer of near-inertial energy below the mixed layer caused by divergence at the coastal boundary). This could explain why some coastal applications of the one-dimensional model find relatively rapid decay constants compared to open ocean values; 9.2 hours [Chen *et al.*, 1996] versus 4–8 days [Pollard and Millard, 1970]. As a result, the evidence for wind forcing during CMO is only qualitative, and no simple quantitative relation between wind stress and near-inertial current variability could be found, although other studies have found evidence for wind forcing to be a primary source of near-inertial variability on the New England shelf [e.g., Wood, 1987].

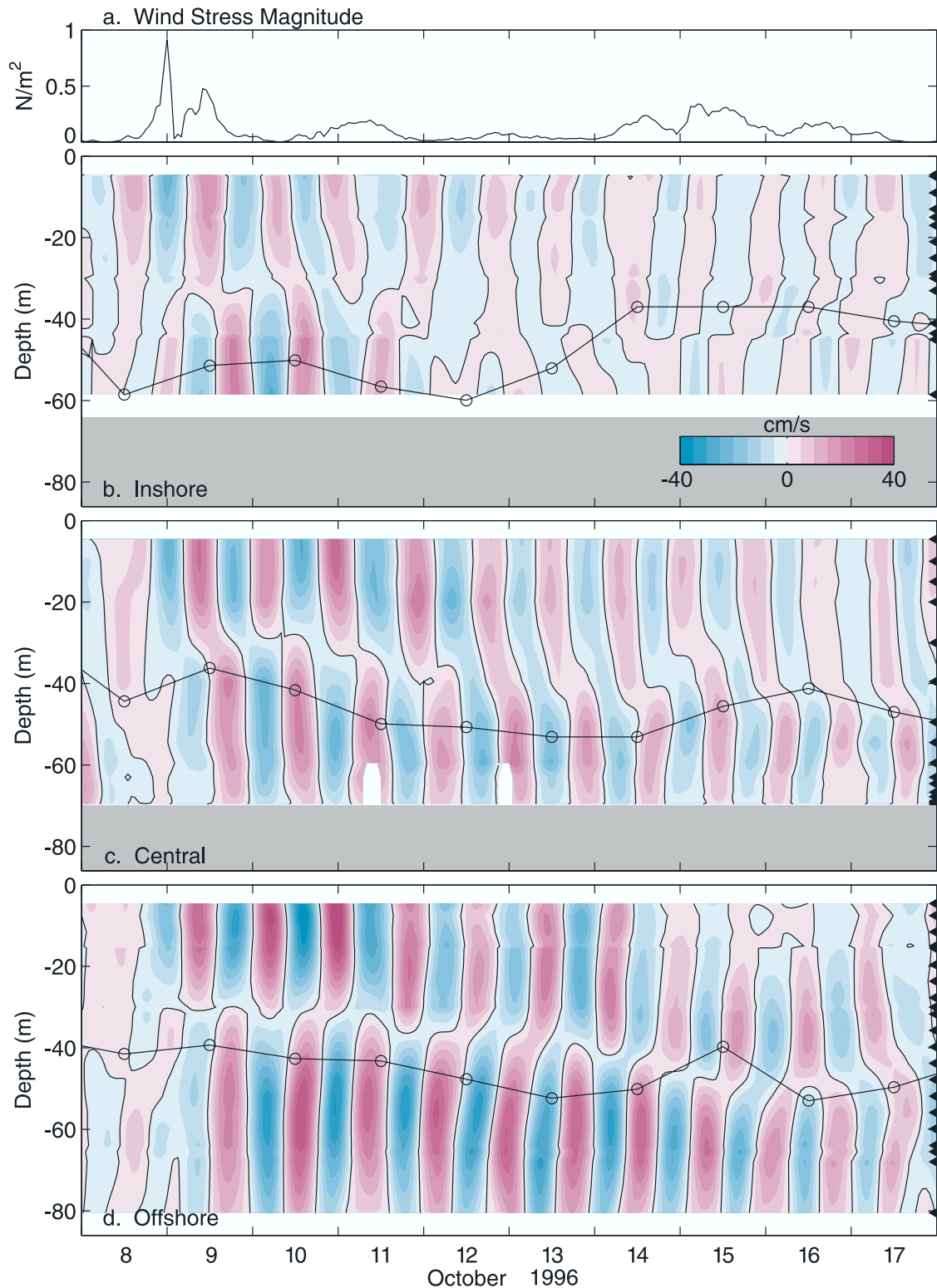


Figure 5. Time series of (a) wind stress magnitude at the central site and eastward current (detided and band-passed) at the (b) inshore, (c) central, and (d) offshore sites. The depth of maximum stratification (daily average) is plotted (circles).

[14] In early October during the CMO experiment, near-inertial current variations are observed directly following a relatively large amplitude burst of wind stress (Figure 5). The early October event exhibits several features common to

CMO near-inertial variability in general. The peak currents range from 20 cm s^{-1} at the inshore site to more than 30 cm s^{-1} at the offshore site, which are larger than the barotropic tides [Moody *et al.*, 1983; Shearman and Lentz,

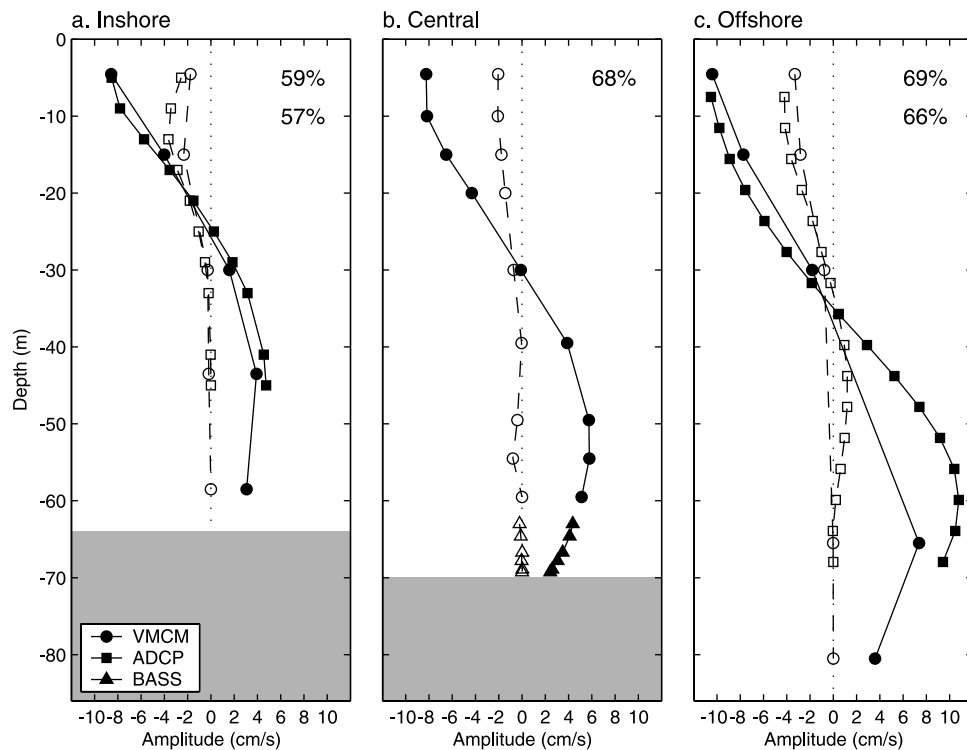


Figure 6. Dominant CEOF, computed from the detided, band-passed (10–33 hours) current observations at the (a) inshore, (b) central, and (c) offshore sites. Real component is indicated by a solid line and solid symbols, while the orthogonal (imaginary) component is indicated by a dashed line and open symbols. The fraction of variance explained is noted (VMCM observations above ADCP).

2004] and as large as many of the subtidal wind-driven current events [Beardsley *et al.*, 1985; Shearman and Lentz, 2003]. The near-inertial currents have a modal vertical structure with one zero-crossing at about 30 m depth, although the zero-crossing depth does vary with the stratification (Figure 5). Near-inertial currents appear highly coherent and approximately in phase from the inshore to offshore sites. Also, current magnitude decreases onshore, and the duration of the early October event decreases from about 9 days at the offshore site to about 5 days at the inshore site. Several other near-inertial events, preceded by a variety of wind-forcing conditions [Baumgartner and Anderson, 1999], are found in the CMO observations with similar cross-shelf dependence on magnitude and duration (Table 1).

3.1. Vertical Structure

[15] The typical vertical structure of near-inertial motions is characterized by complex empirical orthogonal functions

(CEOFs), computed from the detided band-passed current observations at each site. The dominant CEOF (accounting for approximately two thirds of the variance) resembles a first baroclinic mode with maximum values above 10 m, a slight turning of the current vectors with depth above 30 m, one zero-crossing at about 30 m depth, a local maximum at 20–25 meters above bottom (mab), and decreasing values approaching the bottom (Figure 6). At each site, the phase difference between peak upper and lower layer currents is about 160° , consistent with a slight phase lead of about 1 hour in the upper layer (i.e., positive upper layer currents leading negative bottom layer currents). Finally, CEOFs are computed on monthly intervals, during CMO, and the dominant CEOF always resembles a first baroclinic mode, although the structure does vary. The zero-crossings from the monthly CEOFs are significantly correlated (95% confidence level) with monthly estimates of the depth of maximum stratification (0.76) and surface mixed layer

Table 2. Coherence (C) and Relative Phase (ϕ in Degrees) at the Inertial Frequency Between Dominant CEOF (First Baroclinic Mode) Time Series at the Four CMO Mooring Sites^a

Site	Inshore		Central		Offshore		Alongshore	
	C	ϕ	C	ϕ	C	ϕ	C	ϕ
Inshore			0.62	0	0.49	-10	0.60	12
Central	0.60	0			0.75	5	0.89	0
Offshore	0.45	-10	0.70	3			0.69	5
Alongshore	0.54	0	0.77	2	0.55	11		

^aUpper diagonal displays coherence and phase between real components of the CEOF time series, and the lower diagonal displays coherence and phase for the imaginary component.

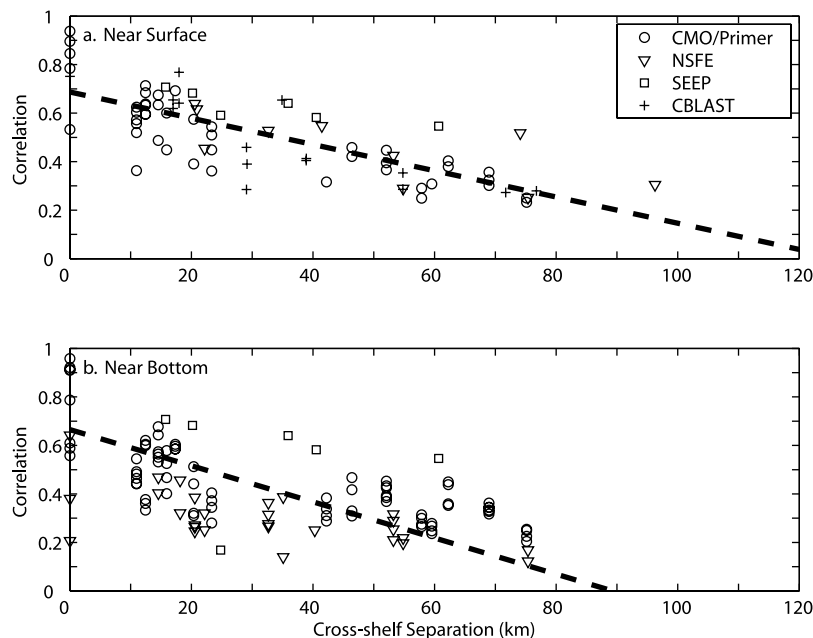


Figure 7. Near-inertial current correlations versus north-south (approximately cross-shelf) separation, computed from the detided, band-passed upper layer (above 20 m) and lower layer (below 30 mab) current meter data from CMO, Shelfbreak Primer, NSFEE, SEEP, and CBLAST. All correlations are significant at the 95% confidence level. Lines fit to correlation data are also shown.

depth (0.61), estimated from the CMO observations of density. For CMO, the baroclinic structure of near-inertial currents has a zero-crossing higher in the water column during more strongly stratified periods (fall and spring) and deeper in the water column during less stratified periods (winter) or when strong stratification appears at deeper levels due to the presence of the foot of the shelf-slope front [Lentz *et al.*, 2003].

3.2. Horizontal Structure

[16] The early-October observations suggest that near-inertial current variability is highly correlated across the CMO array (Figure 5). The full time series of the dominant CEOFs are significantly coherent at near-inertial frequencies among the four CMO mooring sites (maximum separation about 23 km) with near-zero phase differences (Table 2). Furthermore, the cross-shelf decorrelation scale (defined as the first zero-crossing of the correlation function) for the upper layer (above 20 m) near-inertial currents is over 120 km, nearly the width of the entire shelf (Figure 7). The decorrelation scale for the lower layer (0–30 mab) currents is slightly smaller (90 km), but still similar to the full shelf width. The decorrelation scales are computed using the detided, band-passed currents from the CMO and supplementary data sets, and the zero-crossing is determined by fitting a line to the correlation data and extrapolating. The large cross-shelf correlation scale suggests that near-inertial currents are coherent across the entire shelf. A similarly large cross-shelf scale for inertial variability was found using an EOF analysis of the NSFEE current observations [Wood, 1987].

[17] Like near-inertial band variance across the CMO moored array, the dominant CEOF amplitudes decrease in the onshore direction (Figure 6). Furthermore, near-surface

near-inertial band current variance computed from the CMO and supplementary data sets shows that the onshore decrease in near-inertial kinetic energy (one half along-isobath variance plus cross-isobath variance) is a shelf wide feature (Figure 8). Near-inertial energy decreases at a rate of $0.8 \pm 0.2 \text{ cm}^2 \text{ s}^{-2} \text{ km}^{-1}$, estimated from linear regression, from the shelfbreak to about 40.8°N . The larger values north of 40.8°N are due to the fact that the CBLAST data are a

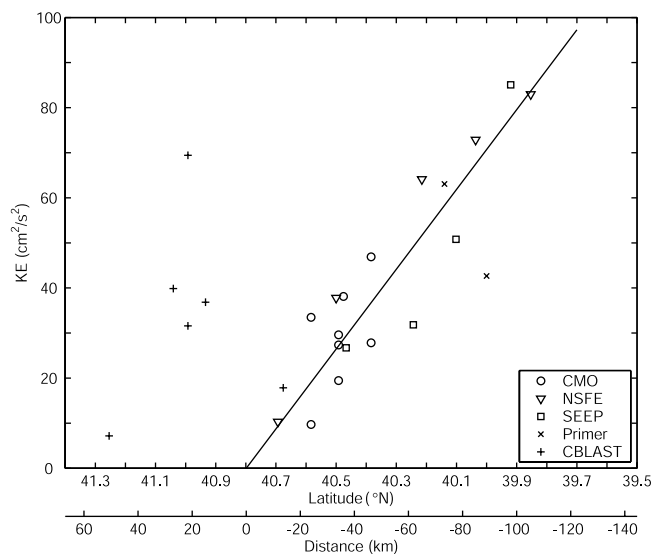


Figure 8. Near-surface (above 20 m) near-inertial kinetic energy, computed from near-inertial band variance of the CMO and supplementary observations, versus latitude across the New England shelf. A line fit to data south of 40.8°N is also shown.

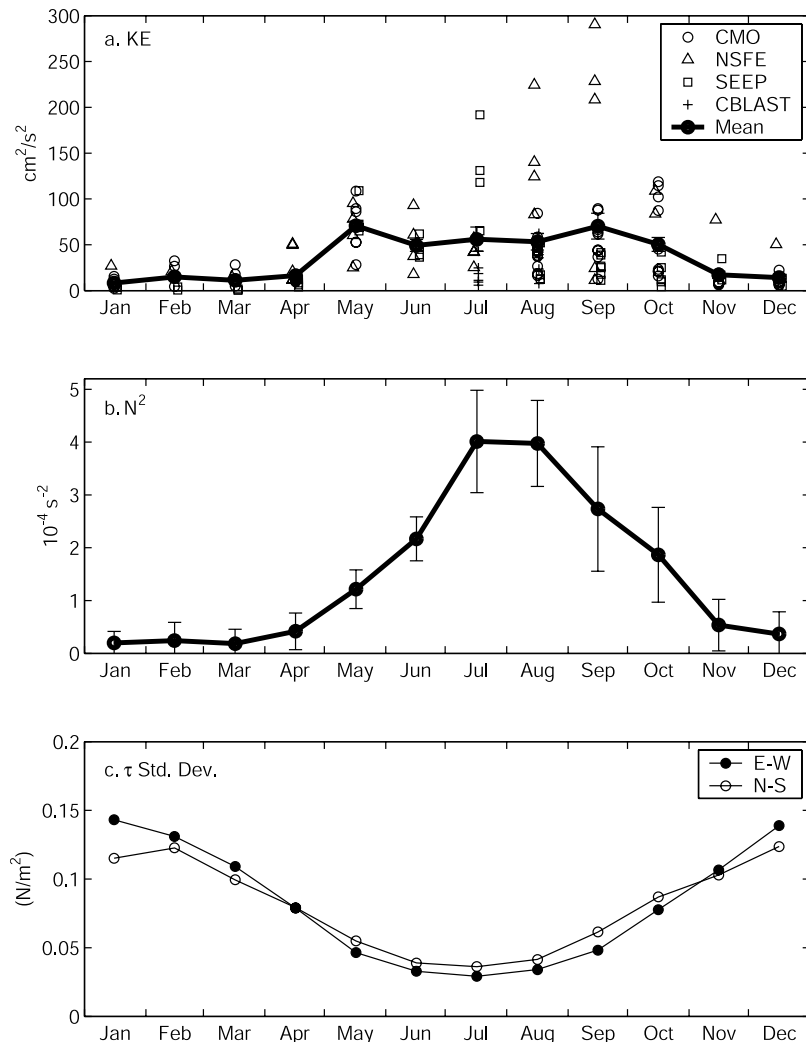


Figure 9. (a) Monthly estimates of near-inertial kinetic energy above 20 m from the CMO and supplemental data sets and the annual cycle (computed as monthly averages), (b) the annual cycle of depth-averaged N^2 over the New England shelf from historical NODC database, and (c) the annual cycle of wind stress variability (monthly standard deviation) estimated from nearby NDBC buoy 440008.

relatively short record during July and August, a peak period for near-inertial variability (see below), while the other records are longer and span a variety of stratification and near-inertial energy conditions. The processes controlling the cross-shelf distribution of near-inertial energy are further examined in section 4.

3.3. Seasonal Variability

[18] Near-inertial current variability is highly episodic, but in general, it tends to be stronger in the summer and weaker in winter (Table 1 and Figure 4). During CMO, the largest amplitude events occur in September, October, and May, while during the winter months, near-inertial variability is consistently weaker. The annual cycle (monthly estimates) of near-surface (above 20 m) near-inertial kinetic energy, computed from near-inertial band variance in the CMO and supplemental current observations, is largest from May through October, following approximately the seasonal cycle in stratification (Figure 9b). The annual cycles of near-inertial kinetic energy and N^2 are highly coherent, while,

conversely, the annual cycle of near-inertial kinetic energy is opposite the annual cycle in wind stress variability (correlation of -0.71). This is seemingly contradictory, since near-inertial variability during CMO appears largely wind forced. This suggests that on average, forcing for near-inertial variability is abundant, even during the summer period of relatively low wind variability.

[19] Ignoring variations in wind-forcing magnitude, a dominant factor controlling the amplitude of the near-surface near-inertial current response is the depth of the surface mixed layer, where an inverse relationship between surface mixed layer depth (SMLD) and near-inertial current amplitude would be expected (i.e., smaller surface mixed layers correspond to larger currents). Furthermore, the annual cycle of surface mixed layer depth will vary inversely in relation to the depth-averaged stratification with higher depth-averaged stratification corresponding to smaller surface mixed layers. Variations in surface mixed layer depth are therefore a potential explanation for the seasonal cycle in near-surface near-

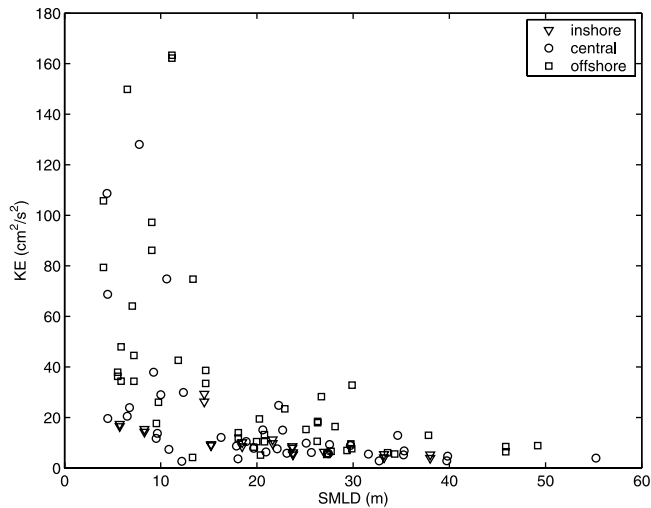


Figure 10. Weekly averages of surface mixed layer depth, during the CMO experiment, versus weekly estimates of near-inertial kinetic energy at 5 m depth from near-inertial band variance. Surface mixed layer depth is estimated from the hourly observations of density [Shearman and Lentz, 2003].

inertial kinetic energy, where kinetic energy is expected to be inversely related to the square of the surface mixed layer depth (i.e., $KE \propto SMLD^{-2}$). During CMO, an inverse relationship is found between weekly estimates of

near-inertial KE (at about 5 m depth) and average surface mixed layer depth at the inshore, central, and offshore sites (Figure 10), with a significant correlation (0.61) between near-inertial KE and $SMLD^{-2}$.

4. Discussion

4.1. Cross-Shelf Distribution of Near-Inertial Kinetic Energy

[20] The observed characteristics of near-inertial current variability on the New England shelf are qualitatively consistent with linear, two-dimensional models of impulsively forced near-inertial variability on a wide, shallow, flat-bottomed shelf [e.g., Millot and Crepon, 1981; Pettigrew, 1981; Kundu et al., 1983; Tintore et al., 1995; Chen et al., 1996]. One of the most significant features of near-inertial current variability in these models is the apparent mode one baroclinic vertical structure, which is the direct result of a surface mixed layer response and barotropic wave emanating from the coastline, and not a true (in the dynamical sense) baroclinic mode [Pettigrew, 1981]. Another significant feature is the ultimately nullifying effect of baroclinic waves emanating from the coastline [Pettigrew, 1981; Kundu et al., 1983].

[21] In the most basic two-layer case, analytical solutions reveal three important phases to the near-inertial current response [see Millot and Crepon, 1981; Pettigrew, 1981]. First, at the onset of forcing (delta or step function), the upper layer responds approximately like the classical one-dimensional homogeneous model, and there is no motion in the lower layer. This phase lasts only a small fraction

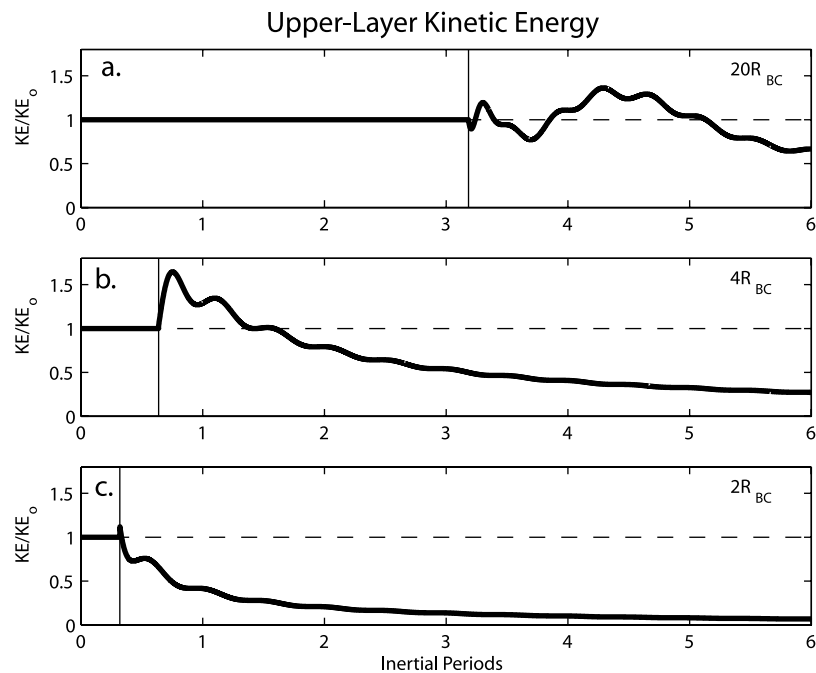


Figure 11. (a,b,c) Temporal evolution of upper-layer kinetic energy at $x = 2, 4,$ and 20 baroclinic deformation radii (R_{BC}), respectively, computed from the analytical solutions to the impulsively forced, two-dimensional, linear, flat bottom coastal wall model [Pettigrew, 1981]. The vertical line marks the arrival of the baroclinic wave. The values kinetic energy are scaled by KE_0 , which is equal to the upper-layer kinetic energy in the limit $x/c_{BC} > t \gg x/c_{BT}$, long after the barotropic wave has passed and before the baroclinic wave has passed.

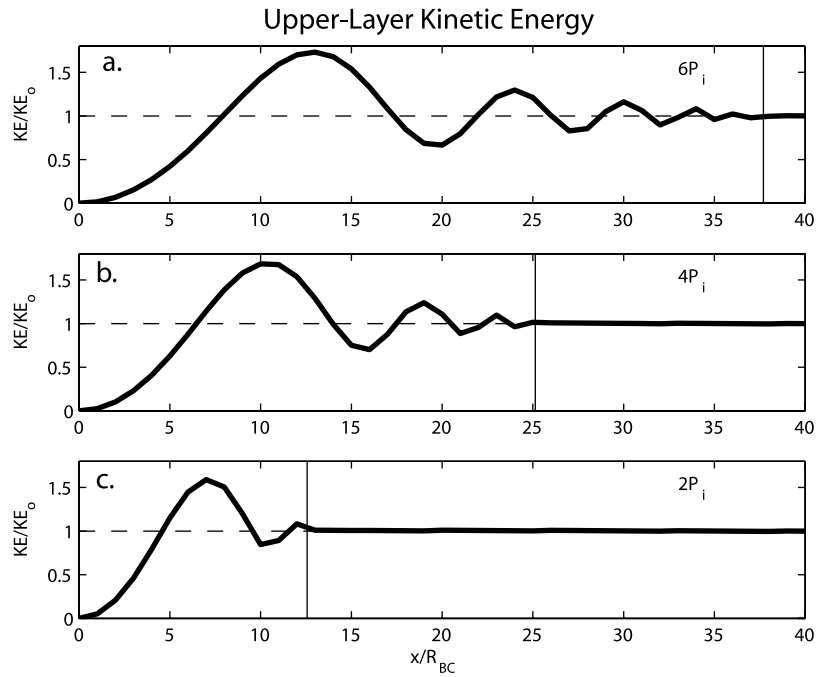


Figure 12. (a, b, c) Spatial distribution of upper-layer kinetic energy after $t = 2, 4,$ and 6 inertial periods, respectively, computed from the analytical solutions to the impulsively forced, two-dimensional, linear, flat bottom coastal wall model [Pettigrew, 1981]. The vertical line marks the arrival of the baroclinic wave. The values kinetic energy are scaled by KE_o , which is equal to the upper-layer kinetic energy in the limit $x/c_{BC} > t \gg x/c_{BT}$, long after the barotropic wave has passed and before the baroclinic wave has passed.

of an inertial period. Barotropic (BT) and baroclinic (BC) waves are generated by divergence at the coastal wall, and propagate offshore. In the second phase, a barotropic wave propagates rapidly out from the coast (e.g., choosing a shelf depth of 70 m yields a barotropic wave speed c_{BT} of about 26 m s^{-1}), covering a typical wide shelf (150 km) in a tiny fraction of an inertial period. After the barotropic wave arrives ($t \gg x/c_{BT}$, where t is time and x is cross-shelf position), the addition of the initial upper layer response and barotropic response results in near-inertial currents with an approximately 180° phase difference between the upper and lower layers. Hence the apparent mode one baroclinic structure. Third, a baroclinic wave propagates more slowly away from the coastline (e.g., choosing upper and lower layer depths of 35 m and a reduced gravity of $g' = 4 \times 10^{-3} \text{ m/s}^2$, yields a baroclinic wave speed c_{BC} of about 0.3 m s^{-1}), modifying the current magnitude and introducing some cross-shelf structure. For $t \gg x/c_{BC}$ (i.e., long after the baroclinic wave has passed), the three components (surface mixed layer, barotropic, and baroclinic) sum to zero [Pettigrew, 1981], nullifying the previously existing near-inertial variability.

[22] For example, near-inertial kinetic energy in the upper layer across the entire shelf rapidly achieves the value

$$KE_o = \frac{1}{2} \left[\frac{\tau_o}{\rho_1 h_1 f \left(1 + \frac{h_1}{h_2} \right)} \right]^2, \quad (1)$$

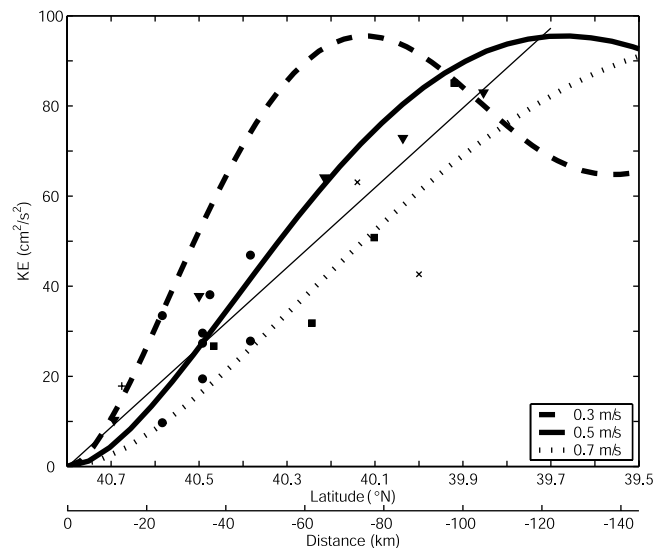


Figure 13. Average cross-shelf distribution of upper-layer near-inertial kinetic energy, estimated from ensembles of events with random magnitude and duration, approximately matching the CMO and supplemental observations, using the analytical solutions to the impulsively forced, two-dimensional, linear, flat bottom coastal wall model [Pettigrew, 1981] with baroclinic wave speeds of 0.3 (long-dashed line), 0.5 (thick solid line), and 0.7 m s^{-1} (short-dashed line), as well as a simple line fit to the observations (thin solid line).

where τ_o is the amplitude of the impulsive wind stress forcing, ρ_1 is the upper layer density, f is the local Coriolis parameter, and h_1 and h_2 are the upper and lower layer depths, respectively (Figure 11). The value KE_o is determined from the analytical solutions for $x/c_{BC} > t \gg x/c_{BT}$ (i.e., long after the barotropic wave has passed and before the baroclinic wave has passed). After the baroclinic wave arrives, near-inertial kinetic energy may increase temporarily, but eventually decays to zero (Figure 11). The spatial distribution of near-inertial kinetic energy is constant in front of the baroclinic wave (Figure 12). In the region behind the baroclinic wave, there is increased spatial variability in magnitude, but the dominant effect is the decrease in magnitude toward the coastline that gradually spreads across the shelf.

[23] Given the similarities between the observed near-inertial currents on the New England shelf and impulsively forced two-dimensional model (i.e., mode one baroclinic structure, large cross-shelf scales), the analytical solutions to the impulsively forced two-layer model are used to examine the observed onshore decrease in the cross-shelf distribution of near-inertial kinetic energy (Figure 8). An ensemble of 2000 near-inertial events with random magnitude (KE_o) and duration are used to compute the mean cross-shelf structure of kinetic energy for different baroclinic wave speeds (0.3, 0.5, and 0.7 m s⁻¹). The random (normally distributed) values for magnitude (mean 60 cm² s⁻², standard deviation 35 cm² s⁻²) and duration (mean 11.5 days, standard deviation 4 days) are chosen to be consistent with the CMO and historical observations. The coastline ($x = 0$) is chosen to match where the linear fit to the observed cross-shelf distribution of near-inertial kinetic energy is zero. The result is an onshore decrease very similar to the observations (Figure 13). The agreement of the observed and modeled near-inertial energy suggests that the average cross-shelf distribution is strongly controlled by how far the erasing baroclinic wave typically gets during a near-inertial event, which is in turn controlled by the propagation speed (stratification) and the duration of an event.

4.2. Effects of Subtidal Flow

[24] A closer inspection of the current spectra shows the broad inertial peak to have substantial variance at subinertial frequencies (Figure 3). To examine the time-dependent frequency content of near-inertial variability, wavelet spectra are computed from the time series of the dominant CEOFs, using a Morlet wavelet (Gaussian times a sinusoid) with a width of 12 periods [e.g., Meyers *et al.*, 1993; Torrence and Compo, 1998]. The time series of the first CEOF at each CMO site is normalized to unit variance, the wavelet power spectrum (wavelet transform amplitude squared) is computed over the near-inertial band with a frequency discretization of 0.01 cpd, and the time-dependent frequency of maximum wavelet power $\omega^{\max}(t)$ is identified. For example, wavelet power at the central site (the other CMO sites are similar) exhibits higher-powered near-inertial events in fall and spring, while winter variability is consistently weak (Figure 14a). In addition, the periods of stronger wavelet power correspond to near-inertial events identified in Table 1. The wavelet analysis (at all four sites) indicates that bursts of near-inertial

Table 3. Linear Regression Slopes and Correlation of Absolute Vorticity ($f + \zeta$) Onto Peak Wavelet Frequency (ω^{\max})^a

	Regression Slope	Correlation
Inshore	1.47 ± 6.50	(0.31)
Inshore ADCP	1.15 ± 2.82	(0.48)
Central	0.99 ± 0.42	0.84
Offshore	0.87 ± 0.54	0.73
Offshore ADCP	0.96 ± 0.97	0.77
Alongshore	0.74 ± 1.38	(0.72)

^aCorrelations not significant at the 95% confidence level are shown in parentheses.

variability during the fall occur at subinertial frequencies, while variability during the spring occurs at the inertial or slightly superinertial frequencies (Figure 14b). Five-day block averaging for ω^{\max} is chosen to match the smoothing of the wavelet transform and the typical duration of a CMO near-inertial event (Table 1), and only periods of relatively strong variance (threshold of 20 times variance) are considered. The accuracy of the wavelet analysis (examined in Appendix A) is about 0.01 cpd, and the results of the wavelet analysis do not qualitatively change for differing wavelet widths (3, 6, 12, and 24 periods), frequency discretization (0.005, 0.01, 0.02, and 0.04 cpd), threshold (20, 40, and 60 times variance), and block averaging (2, 5, 7, and 9 days).

[25] One potential cause for near-inertial motions occurring at subinertial frequencies is through the influence of a mean (or persistent with respect to near-inertial variability) current shear [e.g., Kunze, 1985]. According to Kunze [1985], when the vertical component of relative vorticity (ζ) is a significant fraction of the vertical component of planetary vorticity (f), then it is more appropriate to use the vertical component of absolute vorticity ($f + \zeta$) in determining the local dispersion relation for near-inertial internal waves, yielding an effective Coriolis (inertial) frequency approximated by

$$f_{\text{eff}} = f + \frac{\zeta}{2}. \quad (2)$$

Equation (2) is derived using plane wave solutions for near-inertial internal waves, assuming continuous stratification and internal wave spatial scales approximately equal to or smaller than (WKB approximation) the mean flow scales. The same effective Coriolis frequency results when deriving a dispersion relation for the two-layer, flat-bottom, coastal wall model (now including nonlinear terms).

[26] Owing to the presence of the shelfbreak front (Figure 1), the CMO site is a likely location for large subtidal current shear. The climatology compiled by Linder and Gawarkiewicz [1998] indicates that bi-monthly averages of relative vorticity in the vicinity of the CMO site, associated with cross-shelf shear in the shelfbreak jet, can reach $-0.20f$ [see Linder and Gawarkiewicz, 1998, Figure 16] over approximately 20 km. The CMO fall and spring mean along-isobath flow (Figures 15a and 15b) indicate anticyclonic shear of about $-0.03f$ during the fall and no shear during the spring. Depth-averaged relative vorticity is computed from the CMO subtidal (low-passed with 33 hour cut-off) currents. Gradients are estimated by

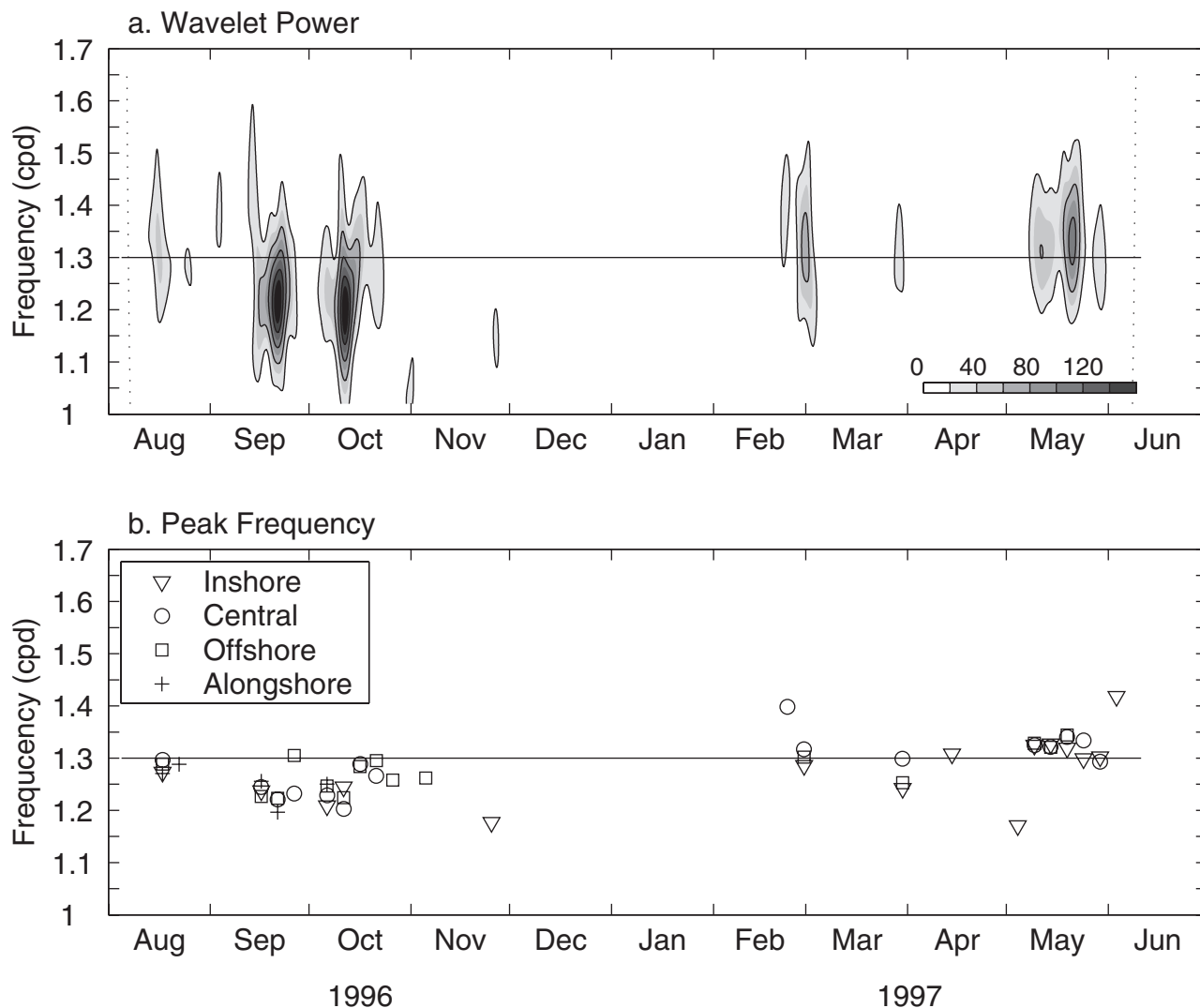


Figure 14. (a) Wavelet power spectrum computed from the real component of the time series (normalized to unit variance) of the first CEOF at the central site. (b) Five-day average of the frequency of peak wavelet power (ω^{\max}) at the four CMO sites.

fitting a plane to the four CMO observations (approximately 20 km separations), following *Shearman and Lenz* [2003], and then depth averaging. Subtidal depth-averaged relative vorticity ranges from $-0.20f$ to $0.15f$, and 5-day averages indicate persistent anticyclonic relative vorticity during the fall and near zero (or slightly cyclonic) during the spring (Figure 15c), consistent with the frequency shift seen in the wavelet spectra (Figure 14b). This is true despite the fact that the spatial scale of the subtidal flow is smaller than the characteristic scale of near-inertial variability, about 20 km for subtidal relative vorticity estimates compared to 100 km for near-inertial variability, a violation of the WKB approximation used in equation (2).

[27] The peak wavelet frequency shows a strong linear relationship to the absolute vorticity $f + \zeta$ (Figure 16). Although the relative vorticity estimate is centered on the CMO central site, comparisons with all four sites are made. Estimates of ω^{\max} and $f + \zeta$ are significantly

correlated at the central and offshore sites (Table 3), and the linear regression slopes are not significantly different from 1. This is puzzling, because it does not agree with the expected result from the dispersion relation (2). Linear regression slopes between ω^{\max} and f_{eff} are 1.97 ± 0.84 and 1.71 ± 1.09 for the central and offshore sites, respectively. The wavelet analysis of peak frequency is highly accurate (see Appendix A), and not a likely reason for the discrepancy.

[28] The strong relationship between ω^{\max} and $f + \zeta$ supports the hypothesis that near-inertial variability is affected by the shear in the subtidal current field on the New England shelf. This has important ramifications for the cross-shelf distribution of near-inertial energy: Near-inertial energy is concentrated in regions of anticyclonic shear [*Kunze*, 1985]. However, no local maximum is seen in the observed cross-shelf distribution of near-inertial kinetic energy (Figure 8). The cross-shelf resolution of the CMO and supplementary data sets is coarse compared

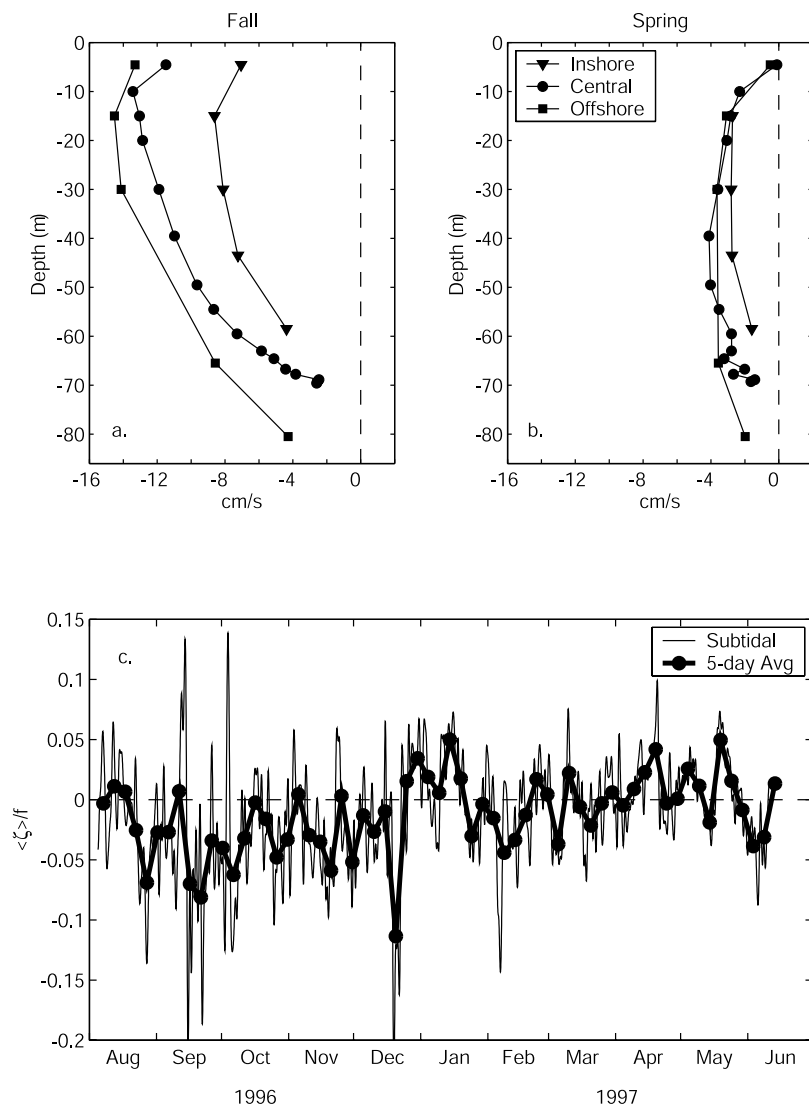


Figure 15. CMO mean along-isobath currents during (a) fall (August–December 1996) and (b) spring (April–June 1997) at the inshore, central, and offshore sites. (c) Subtidal and 5-day averages of depth-averaged relative vorticity (scaled by f), computed from the CMO current observations.

to the scales of the shelfbreak front [Gawarkiewicz *et al.*, 2004], and perhaps with increased resolution, future observations may detect a concentration of near-inertial energy.

5. Conclusions

[29] During CMO, near-inertial current variability on the New England shelf accounts for 10–20% of the total observed current variance (with episodic peak speeds exceeding 30 cm s^{-1}), larger than the variance associated with internal tides or high-frequency internal solitons. Near-inertial current variability is characterized by a mode one baroclinic vertical structure, with a zero-crossing that changes with stratification (stronger stratification corresponds to a shallower zero-crossing). Near-inertial variability is coherent over 20-km scales with no significant phase differences, and has a large (100 km) cross-shelf correlation scale suggesting that near-inertial motions are

coherent across the entire shelf. The amplitude and duration of individual near-inertial events decrease in the onshore direction, and so does the total near-inertial variance. Seasonally, near-surface near-inertial kinetic energy is large from May through October, following approximately the seasonal variation in stratification and opposite to the seasonal cycle in wind stress variance.

[30] Near-inertial current variance on the New England shelf has several features in common with impulsively forced, two-dimensional, flat bottom coastal wall models of near-inertial variability; low mode baroclinic vertical structure (resulting from the sum of a mixed layer response and barotropic response, and not an actual internal wave), large cross-shelf scales, and near-surface near-inertial kinetic energy inversely related to the surface mixed layer depth. The observed onshore decrease in near-inertial energy is similar to the decrease predicted by the simple two-layer model of Pettigrew [1981]. In this model, the primary physical process responsible for this decrease is a

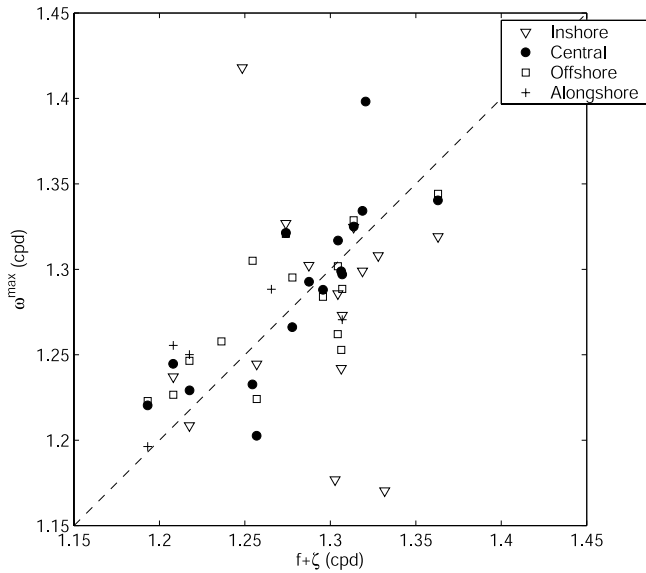


Figure 16. Comparison of absolute vorticity ($f + \zeta$) and peak wavelet frequency (ω^{\max}) at the inshore, central, offshore, and alongshore sites. The dashed line has a slope of 1.

baroclinic wave propagating away from the coast. The agreement between observed and modeled cross-shelf distributions of near-inertial kinetic energy suggests the importance of the baroclinic wave and its ultimately negating effects on the New England shelf. Finally, near-inertial variability over the New England shelf is affected by the subtidal relative vorticity field. During the fall when relative vorticity at the CMO site is persistently anticyclonic, near-inertial motions occur at subinertial frequencies. The wavelet identified peak frequency ω^{\max} is significantly correlated and linearly related (with a slope of 1) to the absolute vorticity $f + \zeta$, which does not agree with the expected relationship from the dispersion relation.

Appendix A: Accuracy of the Wavelet Analysis

[31] Several steps were taken to estimate the accuracy of the wavelet analysis and the ability to identify the peak wavelet frequency (ω^{\max}). First, for several bursts of near-inertial variability during CMO, the oscillation period was estimated simply by determining the time interval between maxima and minima in the detided, band-passed current observations. The 5-day average of period from peak wavelet frequency and a similar average of the simply estimated period agree to within approximately 15 min.

[32] A more rigorous test was then devised to test the ability of the wavelet analysis to identify peak period. A time series was generated from a random assemblage of concurrently running near-inertial signals of the form

$$x^n = A^n \sin(\omega^n \Delta t^n + \phi^n), \quad (\text{A1})$$

where Δt^n is a random duration chosen to have a mean of 5 days and a standard deviation of 1 day over all n , A^n is a random amplitude with a mean of 1.0 and standard deviation of 0.2, ω^n is the frequency of interest and is chosen to have a normal random distribution with a mean of 1.3 cpd and standard deviation of 0.1 cpd, and ϕ^n is a uniformly distributed random phase. The time series (x) is the concatenation of all n events, in this case $n = 10,000$. Next, random noise with standard deviation of 1.0 and a red spectrum is added to the time series. The wavelet analysis was then applied to the test time series, using parameters that match the application to the CMO data, and 5-day averages of the wavelet identified peak frequency were compared to averages of ω^n via linear regression. The correlation between 5-day averages of ω^{\max} and ω^n is high (0.98), and the linear regression slope is 1.00 ± 0.01 (Figure A1), indicating that the wavelet analysis is accurate to within about ± 0.01 cpd.

[33] In addition, fundamental parameters (wavelet width, threshold level, block-averaging duration, and noise level) were varied to examine the sensitivity of the wavelet analysis. The best results were achieved when block-averaging duration was approximately equal to the average near-inertial event duration. Less sensitive was the wavelet width, but results were slightly better when wavelet width and mean duration were approximately equal. Also, threshold level was important. Setting a level of 1.4 times the mean event amplitude effectively removes the periods when the wavelet analysis samples two separate events, and thus improves the overall accuracy. Finally, noise amplitude and spectral characteristics (red or white) have very little overall effect on the ability of the wavelet analysis to identify peak frequency.

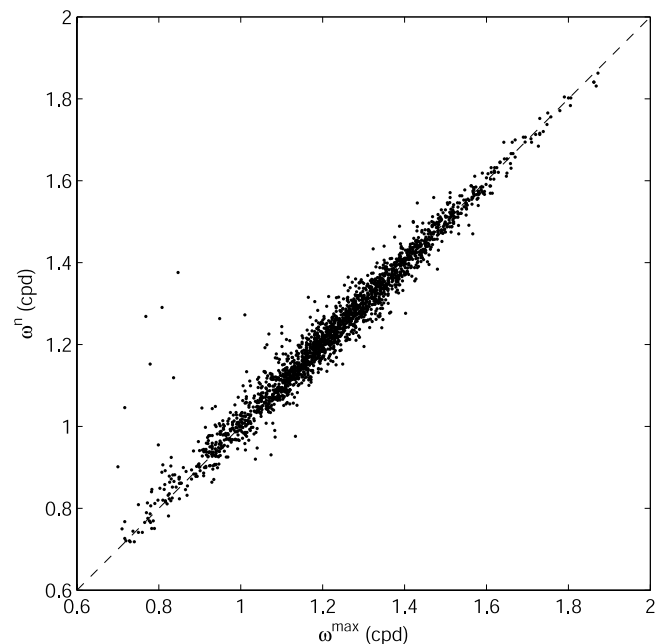


Figure A1. Comparison of 5-day averages of the peak wavelet frequency (ω^{\max}) and test signal frequency (ω^n). The dashed line has a slope of 1.

[34] **Acknowledgments.** I thank N. Galbraith, W. Ostrom, R. Payne, R. Trask, G. Tupper, J. Ware, and B. Way of the WHOI Upper Ocean Processes Group and the WHOI Rigging Shop under the direction of D. Simoneau with assistance from M. Baumgartner, C. Marquette, Lt. M. Martin, N. McPhee, E. Terray, and S. Worrilow for the design, deployment, and recovery of the moored array, the preparation of the instruments, and processing of the data. Also, I am grateful for the contributions of S. Lentz, A. Plueddmann, K. Polzin, D. Chapman, K. Brink, C. Lee, J. Lerczak, J. Edson, and two anonymous reviewers. Funding for the CMO experiment and subsequent analysis was provided by the Office of Naval Research under grants N00014-95-1-0339 and N00014-01-1-0140.

References

- Aikman, F., III, H. W. Ou, and R. W. Houghton (1988), Current variability across the New England continental shelf-break and slope, *Cont. Shelf Res.*, *8*, 625–651.
- Baumgartner, M. F., and S. P. Anderson (1999), Evaluation of NCEP regional weather prediction model surface fields over the Middle Atlantic Bight, *J. Geophys. Res.*, *104*, 18,141–18,158.
- Beardsley, R. C. (1987), A comparison of the vector-averaging current meter and New Edgerton, Germeshausen, and Grier, Inc., vector-measuring current meter on a surface mooring in Coastal Ocean Dynamics Experiment 1, *J. Geophys. Res.*, *92*, 1845–1860.
- Beardsley, R. C., D. C. Chapman, K. H. Brink, S. R. Ramp, and R. Schlitz (1985), The Nantucket Shoals Flux Experiment (NSFE79): I. A basic description of the current and temperature variability, *J. Phys. Oceanogr.*, *15*, 713–748.
- Bigelow, H. B. (1933), Studies of the waters on the continental shelf, Cape Cod to Chesapeake Bay: I. The cycle of temperature, *Pap. Phys. Oceanogr. Meteorol.*, *2*, 1–135.
- Chant, R. J. (2001), Evolution of near-inertial waves during an upwelling event on the New Jersey inner shelf, *J. Phys. Oceanogr.*, *31*, 746–764.
- Chen, C., R. O. Reid, and W. D. Nowlin Jr. (1996), Near-inertial oscillations over the Texas-Louisiana shelf, *J. Geophys. Res.*, *101*, 3509–3524.
- Dickey, T. D., and A. J. Williams III (2001), Interdisciplinary ocean process studies on the New England shelf, *J. Geophys. Res.*, *106*, 9427–9434.
- Federik, J., and J. S. Allen (1996), Model studies of near-inertial waves in flow over the Oregon continental shelf, *J. Phys. Oceanogr.*, *26*, 2053–2075.
- Fratantoni, P. S., and R. S. Pickart (2003), Variability of the shelfbreak jet in the Middle Atlantic Bight: Internally or externally forced?, *J. Geophys. Res.*, *108*(C5), 3166, doi:10.1029/2002JC001326.
- Galbraith, N., A. Plueddemann, S. Lentz, S. Anderson, M. Baumgartner, and J. Edson (1999), Coastal Mixing and Optics experiment moored array data report, *Tech. Rep. WHOI-99-15*, Woods Hole Oceanogr. Inst., Woods Hole, Mass.
- Gawarkiewicz, G., F. Bahr, K. H. Brink, R. C. Beardsley, M. Caruso, and J. Lynch (2004), A large-amplitude meander of the shelfbreak front during summer south of New England: Observations from the Shelfbreak PRIMER Experiment, *J. Geophys. Res.*, *109*, C03006, doi:10.1029/2002JC001468.
- Islen, C. O. (1936), A study of the circulation of the western North Atlantic, *Pap. Phys. Oceanogr. Meteorol.*, *4*, 687–710.
- Kundu, P. K. (1976), An analysis of inertial oscillations observed near the Oregon coast, *J. Phys. Oceanogr.*, *6*, 879–893.
- Kundu, P. K., S.-Y. Chao, and J. P. McCreary (1983), Transient coastal currents and inertio-gravity waves, *Deep Sea Res.*, *30*, 1059–1082.
- Kunze, E. (1985), Near-inertial wave propagation in geostrophic shear, *J. Phys. Oceanogr.*, *15*, 544–565.
- Lentz, S. J., R. K. Shearman, S. Anderson, A. J. Plueddmann, and J. Edson (2003), The evolution of stratification over the New England shelf during the Coastal Mixing and Optics study, August 1996 to June 1997, *J. Geophys. Res.*, *108*(C1), 3008, doi:10.1029/2001JC001121.
- Lerczak, J. A., M. C. Hendershott, and C. D. Winant (2001), Observations and modeling of coastal internal waves driven by a diurnal sea breeze, *J. Geophys. Res.*, *106*, 19,715–19,729.
- Linder, C. A., and G. Gawarkiewicz (1998), A climatology of the shelf-break front in the Middle Atlantic Bight, *J. Geophys. Res.*, *103*, 18,405–18,423.
- Martin, M. J. (1998), An investigation of momentum exchange parameterizations and atmospheric forcing for the Coastal Mixing and Optics program, Master's thesis, Mass. Inst. of Technol./Woods Hole Oceanogr. Inst., Woods Hole, Mass.
- Mayer, D. A., H. O. Mofjeld, and K. D. Leaman (1981), Near-inertial internal waves observed on the outer shelf in the Middle Atlantic Bight in the wake of Hurricane Belle, *J. Phys. Oceanogr.*, *11*, 87–106.
- Meyers, S. D., G. G. Kelly, and J. J. O'Brien (1993), An introduction to wavelet analysis in oceanography and meteorology: With application to the dispersion of yanai waves, *Mon. Weather Rev.*, *121*, 2858–2866.
- Millot, C., and M. Crepon (1981), Inertial oscillations on the continental shelf of the Gulf of Lions—Observation and theory, *J. Phys. Oceanogr.*, *11*, 639–657.
- Moody, J. A., et al. (1983), Atlas of tidal elevation and current observations on the northeast American continental shelf and slope, *U.S. Geol. Serv. Bull.*, *1161*, 122 pp.
- Pettigrew, N. R. (1981), The dynamics and kinematics of the coastal boundary layer off Long Island, Ph.D. thesis, Mass. Inst. of Technol./Woods Hole Oceanogr. Inst., Woods Hole, Mass.
- Pollard, R. T. (1970), On the generation by winds of internal waves in the ocean, *Deep Sea Res.*, *17*, 795–812.
- Pollard, R. T. (1980), Properties of near surface inertial oscillations, *J. Phys. Oceanogr.*, *10*, 387–398.
- Pollard, R. T., and R. C. Millard Jr. (1970), Comparison between observed and simulated wind-generated inertial oscillations, *Deep Sea Res.*, *17*, 813–821.
- Shaw, W. J., J. H. Trowbridge, and A. J. Williams III (2001), Budgets of turbulent kinetic energy and scalar variance in the continental shelf bottom boundary layer, *J. Geophys. Res.*, *106*, 9551–9564.
- Shearman, R. K., and S. J. Lentz (2003), Dynamics of mean and subtidal flow on the New England shelf, *J. Geophys. Res.*, *108*(C8), 3281, doi:10.1029/2002JC001417.
- Shearman, R. K., and S. J. Lentz (2004), Observations of tidal variability on the New England shelf, *J. Geophys. Res.*, *109*, C06010, doi:10.1029/2003JC001972.
- Tintore, J., D.-P. Wang, E. Garcia, and A. Viudez (1995), Near-inertial motions in the coastal ocean, *J. Mar. Syst.*, *6*, 301–312.
- Torrence, C., and G. P. Compo (1998), A practical guide to wavelet analysis, *Bull. Am. Meteorol. Soc.*, *79*, 61–78.
- Weller, R. A., T. Farrar, L. Hutto, C. Zappa, and D. L. Thompson (2003), Spatial and temporal scales of oceanic variability in the CBLAST-Low study region, *Eos Trans. AGU*, *84*(46), Ocean Sci. Meet. Suppl., Abstract OS51G-03.
- Williams, A. J., III, J. S. Tochko, R. L. Koehler, W. D. Grant, T. F. Gross, and C. V. R. Dunn (1987), Measurement of turbulence in the oceanic bottom boundary layer with an acoustic current meter array, *J. Atmos. Oceanic Technol.*, *4*, 312–327.
- Wood, T. M. (1987), Observations of inertial oscillations during the Nantucket Shoals Flux Experiment, Master's thesis, Mass. Inst. of Technol./Woods Hole Oceanogr. Inst., Woods Hole, Mass.
- Young, W. R., and M. Ben Jelloul (1997), Propagation of near-inertial oscillations through a geostrophic flow, *J. Mar. Res.*, *55*, 735–766.

R. K. Shearman, Department of Physical Oceanography, Woods Hole Oceanographic Institution, Woods Hole, MA 02543, USA. (kshearman@whoi.edu)